Strained-Germanium Nanostructures for Infrared Photonics

Cicek Boztug,[†] José R. Sánchez-Pérez,[‡] Francesca Cavallo,[‡] Max G. Lagally,[‡] and Roberto Paiella[†,*]

[†]Department of Electrical and Computer Engineering and Photonics Center, Boston University, Boston, Massachusetts 02215, United States and [‡]Department of Materials Science and Engineering, University of Wisconsin—Madison, Madison Wisconsin 53706, United States

ABSTRACT The controlled application of strain in crystalline semiconductors can be used to modify their basic physical properties to enhance performance in electronic and photonic device applications. In germanium, tensile strain can even be used to change the nature of the fundamental energy band gap from indirect to direct, thereby dramatically increasing the interband radiative efficiency and allowing population inversion and optical gain. For biaxial tension, the required strain levels (around 2%) are physically accessible but necessitate the use of very thin crystals. A particularly promising materials platform in this respect is provided by Ge nanomembranes, that is, single-crystal sheets with nanoscale thicknesses that are either completely released from or partially suspended over their native substrates. Using this approach, Ge tensilely strained beyond the expected threshold for direct-band gap behavior has recently been demonstrated, together with strong strain-enhanced photoluminescence and evidence of population inversion. We review the basic properties, state of the art, and prospects of tensilely strained Ge for infrared photonic applications.

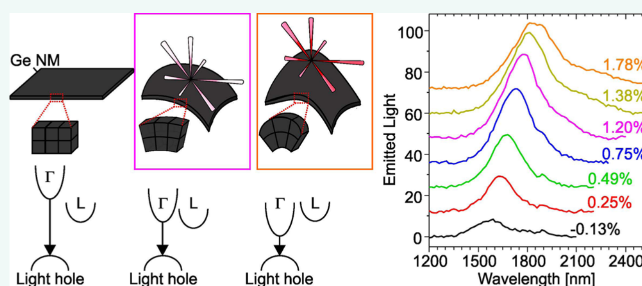

KEYWORDS: germanium · strain engineering · semiconductor nanomembranes · group-IV semiconductor photonics · infrared optoelectronics · nanofabrication · luminescence · optical gain media

Germanium, a group-IV semiconductor, offers a wide range of established and potential technological applications of high relevance and impact. In microelectronics, the large mobility of both electrons and holes in bulk Ge is attractive for the purpose of increasing the speed and drive current of CMOS-based logic devices.[1] Traditionally, the widespread development of Ge metal–oxide–semiconductor field-effect transistors (MOSFETs) has been limited by the lack of a stable native oxide for gate insulation (in contrast to SiO_2 on Si). The recent focus on high-k dielectrics as a means to enable continued device miniaturization has, however, opened the door to potential high-mobility replacements for Si as the channel material, and among these, Ge has the advantage of direct CMOS compatibility. In optoelectronics, Ge is already a well-established photodetector material for use in on-chip data distribution, thanks to its strong interband absorption at near-infrared optical communication wavelengths and, again, to its direct compatibility with the Si microelectronics platform.[2] Additional applications within the emerging field of group-IV photonics, including light emitters,[3] lasers,[4] and solar cells,[5] are being widely investigated.

As in other crystalline semiconductors, the transport and optical properties of Ge can be engineered to enhance device performance through the controlled introduction of strain. The underlying idea is that the electronic band structure of a semiconductor crystal, which determines its key measurable properties, depends not only on the chemical nature of the constituent atoms but also on their spatial arrangement, which in turn is directly modified by the presence of strain. Strain can be used to lift degeneracies in the band structure at high-symmetry points of reciprocal space, thereby suppressing intervalley and interband scattering, and to modify the curvature of energy bands near their extrema and therefore the effective masses relevant to electronic transport. These ideas have already

* Address correspondence to rpaiella@bu.edu.

Received for review September 9, 2013 and accepted March 5, 2014.

Published online March 05, 2014
10.1021/nn404739b

© 2014 American Chemical Society

REVIEW

been widely applied to group-IV semiconductors (including Ge as well as Si and SiGe) to produce significant carrier mobility enhancements, leading to improved MOSFET performance.[6,7]

Particularly remarkable for Ge is that strain can also be used to modify the very nature of its fundamental energy band gap, leading to a dramatic change in its optical radiative properties. As is well known, unstrained Ge is an indirect-band gap semiconductor, with the valence band maxima occurring at the Γ point of reciprocal space (where the crystal wave vector **k** is zero), whereas the conduction band has four degenerate absolute minima at the L points (*i.e.*, on the boundaries of the first Brillouin zone along the ⟨111⟩ directions). Electron–hole recombination between these band extrema involves a very large change in the electronic momentum $\hbar\mathbf{k}$ that cannot be simply transferred to a photon, as photons carry negligible momentum compared to carriers in a semiconductor. As a result, unstrained Ge is an extremely inefficient light emitter. At the same time, a local conduction band minimum also exists at the Γ point, which can be lowered in energy relative to the L valleys through the application of tensile strain until (around 2% biaxial strain) Ge becomes a direct-band gap material.[8] This behavior is illustrated in Figure 1a,b, which shows schematically the band structures of unstrained Ge and Ge under 1.9% biaxial tensile strain, respectively. In other words, the band structure of Ge is so sensitive to the interatomic separation that, if the lattice is made about 2% larger, the band edges move sufficiently (and differentially) so that the minimum at the Γ point becomes the absolute conduction band minimum. Under these conditions, a large fraction of the electrons in the conduction band resides near the Γ point, where they can efficiently recombine with the holes in the corresponding $\mathbf{k} = 0$ valence band maxima *via* light emission. The difficulty, of course, is that a bulk piece of Ge cannot be strained nearly that much without fracturing. This article reviews the approaches that have been used to strain Ge and the optical properties of the resulting materials that have been obtained.

The phenomenon just described represents a particularly striking manifestation of the power of strain engineering in solid-state science and technology. From an application standpoint, it has important potential implications in the ongoing search for a practical Si-compatible laser technology that can be integrated seamlessly with CMOS microelectronics.[9] Such a technology, combined with the already existing suite of group-IV optoelectronic devices, would allow for the complete integration of electronic and photonic functionalities on the same chip, for applications ranging from clock and signal distribution in microprocessors to lab-on-a-chip systems for biochemical sensing, imaging, and LIDAR (laser imaging detection and ranging). The promise of tensilely strained Ge in this context has been known for several years, based on extensive theoretical studies.[10−18] At the same time, however, the introduction of the required levels of tensile strain has until recently remained inaccessible.

VOCABULARY: **biaxial tension** - tensile stress introduced in a crystal in two orthogonal directions; **CMOS** - complementary metal–oxide–semiconductor, a technology for developing integrated electronic circuits; **deformation potential** - a material parameter that quantifies the change in the energy states of an electron in a crystal (*e.g.*, in the conduction or valence bands) caused by an elastic deformation of the crystal structure; **degenerately doped semiconductor** - a semiconductor with such a high level of doping that it starts to act more like a metal than as a semiconductor; **direct/indirect-band gap** - a semiconductor or insulator has a direct energy band gap if the minimum of the conduction band and the maximum of the valence bands (respectively, the lowest unoccupied and the highest fully occupied energy bands in thermal equilibrium at low temperature) occur at the same value of the electronic crystal momentum. Otherwise, the crystal is said to have an indirect-band gap; **heteroepitaxy** - the deposition of a crystalline overlayer on a crystalline substrate of a different material, in which there is registry between the overlayer and the substrate; **nanomembrane** - a single-crystal sheet with thickness on the order of 5–500 nm that is completely released from or partially suspended over its rigid support; **optical gain** - the ability of a physical system (in the presence of population inversion) to amplify the intensity of an optical wave propagating through the system; **optoelectronic device** - a semiconductor structure that acts as an electrical-to-optical or optical-to-electrical transducer to emit, detect, or control light; **plastic relaxation** - irreversible deformation of a material when a threshold load level is reached; **population inversion** - a physical system (such as a group of atoms or molecules or a crystal) that contains a higher density of constituent elements in an excited state than in a lower-energy state. A population inversion is a necessary ingredient in the workings of a standard laser; **radiative recombination efficiency** - the probability that an electron–hole pair in a semiconductor recombines through the emission of light, as opposed to some non-radiative mechanism; **stressor material** - a material deposited on top of another for the purpose of introducing mechanical stress; **transparency carrier density** - the density of electrons and holes in a semiconductor for which the optical absorption and emission rates due to transitions between the conduction and valence bands are equal to each other. A population inversion is established when the semiconductor is pumped above transparency (*i.e.*, when the carrier density exceeds the transparency value); **transverse magnetic (TM) and transverse electric (TE) light** - linearly polarized light with magnetic and electric field, respectively, perpendicular to the plane of incidence toward a planar dielectric interface.

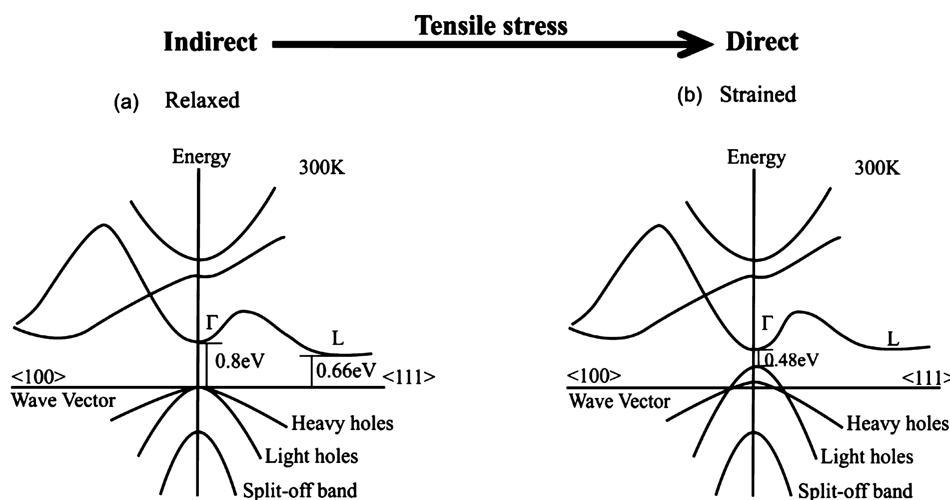

Figure 1. Strain-induced modifications of the Ge band structure. (a) Schematic band structure of unstrained Ge. (b) Schematic band structure of Ge under 1.9% biaxial tensile strain in a {100} plane.

The traditional approach of heteroepitaxy is not immediately applicable, as the most commonly used growth templates for Ge (*i.e.*, compositionally graded SiGe layers grown on Si) have smaller in-plane lattice constants and therefore produce compressively rather than tensilely strained Ge epilayers. The growth of Ge on different templates, including InGaAs[19−21] and SiGeSn,[11,22] has recently been investigated to create tensile strain in Ge. At the same time, alternative methods for straining Ge, based on the application of mechanical stress *via* external forces,[23−26] mechanical grinding of nanocrystals,[27] or the use of suitable stressor layers,[28−34] have been developed.

Regardless of the straining mechanism, the Ge layer thickness and the achievable strain beyond which the structure irreversibly relaxes *via* plastic deformation and cracking are correlated. With heteroepitaxy, sufficiently thin films can readily be produced by simply controlling the growth time. For externally applied stress, Ge nanomembranes (NMs) must be employed, that is, single-crystal sheets with thicknesses of only a few tens of nanometers that are either completely released from or partially suspended over their native rigid substrate.[35] In recent work, Ge NMs have been mechanically strained beyond the accepted threshold for direct-band gap behavior, leading to strong strain-enhanced luminescence and evidence of population inversion under optical pumping.[25] The applied strain is biaxial, an important consideration.

The structure of this article is as follows. We first describe the key features of the Ge electronic band structure under different straining conditions, both biaxial and uniaxial. Next, we review the straining techniques that have been employed in order to improve the Ge radiative recombination efficiency. To illustrate relevant materials issues, we discuss mechanically stressed NMs in somewhat more detail. The optical properties of tensilely strained Ge are then described, including numerical calculations of the expected gain coefficient as a function of strain and experimental data of strain-enhanced light emission. The key challenges and prospects for the development of strain-enabled Ge NM photonic devices are briefly discussed in the concluding section.

Strain Engineering of the Ge Band Structure. In this section, we describe how the electronic band structure of bulk Ge can be modified through the controlled introduction of strain. The key outcome is that all conduction band minima move lower in absolute energy with increasing tensile strain, but the direct minimum at the Γ point moves more rapidly compared to the L valleys, so that, at sufficiently large strain, Ge becomes a direct band gap semiconductor. For uniform expansion in all directions (*i.e.*, purely hydrostatic tensile strain), the transition from indirect to direct-band gap behavior occurs at a relatively small strain of about 0.8%. Hydrostatically tensilely straining a material is not practical, however, and so tensile strain in a crystal is generally introduced either along one crystallographic direction (uniaxial strain) or isotropically on a plane (biaxial strain). In bi- and uniaxially strained materials, both the change in volume (hydrostatic strain) and the change in shape (distortional strain) affect the band structure. Specifically, hydrostatic and distortional strain applied in one, two, or three dimensions produces different changes in the band structure. As a result, because of the changing balance between the hydrostatic and distortional components of strain in uniaxially and biaxially strained materials, the tensile strain required to move the bands sufficiently to achieve direct-band gap Ge is highest in general for uniaxial strain, followed by biaxial strain. The most favorable practical configuration is that of biaxial tensile strain in a {100} plane, where a strain threshold of less than 2% is estimated.[10−13,15−18] For uniaxial stress, the required strain is generally computed to be more

than 4%. Biaxial and uniaxial strains also cause a splitting of the heavy hole (HH) and light hole (LH) valence bands at the Γ point and a concomitant modification of the effective masses of holes in these bands. Such modifications have important practical consequences for electrical and optical properties. The valence band edge at the Γ point (which always remains as the absolute valence band maximum) also moves up in energy with tensile strain, which, combined with the downward motion of the conduction band edge, leads to a narrowing of the band gap. This behavior can be clearly seen in the schematic band diagrams of Figure 1.

Conduction Band Edges. The results just discussed can be derived and quantified using standard deformation potential theory.[36] In this framework, the conduction band minima at the Γ and L points can be written as

$$E_{\Gamma} = E_{\Gamma}^{(0)} + a_{c}(\varepsilon_{xx} + \varepsilon_{yy} + \varepsilon_{zz}) \quad (1)$$

$$E_{L} = E_{L}^{(0)} + \left(\Xi_{d} + \frac{1}{3}\Xi_{u}\right)(\varepsilon_{xx} + \varepsilon_{yy} + \varepsilon_{zz}) \quad (2)$$

where the superscript (0) refers to the unstrained values, a_c and $\Xi_d + 1/3\Xi_u$ are the relevant hydrostatic deformation potentials, and ε_{xx}, ε_{yy}, and ε_{zz} are the diagonal elements of the strain tensor (relative to the system of coordinates defined by the crystal basis vectors). All off-diagonal strain elements here are taken to be zero [otherwise additional terms would appear in eq 2], which is appropriate for all straining configurations considered in this review. The important property that allows for the formation of direct-band gap Ge under tensile strain is that, while both a_c and $\Xi_d + 1/3\Xi_u$ are negative, $|a_c|$ is significantly larger than $|\Xi_d + 1/3\Xi_u|$. Specifically, in the calculations summarized in this review, a value of −8.24 eV is used for a_c, based on the theoretical study of ref 37, which appears to be in good agreement with the measured pressure dependence of the Ge direct-band gap.[11,38] For $\Xi_d + 1/3\Xi_u$, a value of −2.34 eV is used, as recommended in ref 11, based on the measured pressure dependence of the indirect-band gap.[39] The energy separation between the Γ- and L-conduction band minima in unstrained Ge, $E_{\Gamma}^{(0)} - E_{L}^{(0)}$, is well-established at about 140 meV.[40]

For purely hydrostatic strain, we have $\varepsilon_{xx} = \varepsilon_{yy} = \varepsilon_{zz} \equiv \varepsilon$, and the strain threshold for direct-band gap behavior can be obtained by setting E_{Γ} and E_L from eqs 1 and 2 equal to each other and then solving the resulting equation for ε. The result is 0.8%, as already mentioned. In the realistic case of biaxial strain in a {100} plane, only the in-plane diagonal elements of the strain tensor are equal to each other (*e.g.*, $\varepsilon_{xx} = \varepsilon_{yy} \equiv \varepsilon$). Specifically, if the strain is introduced *via* pseudomorphic heteroepitaxy, the parameter ε is given by the fractional difference between the unstrained in-plane lattice constants of the epitaxial film material and the growth template. If the strain is produced through the application of external stress, ε is linearly related to the applied biaxial tension. In either case, the remaining diagonal element of the strain tensor, ε_{zz}, can then be obtained from the requirement that the stress component in the out-of-plane direction must be zero in equilibrium, leading to the relationship

$$\varepsilon_{zz} = -2\frac{C_{12}}{C_{11}}\varepsilon \quad (3)$$

where C_{11} and C_{12} are elastic stiffness constants. Under these conditions, E_{Γ} becomes equal to E_L at a strain level ε of about 1.9% if the Ge material parameters listed in Table 1 are used. It should be noted that the {100} biaxial tensile strain threshold for direct-band gap Ge has been computed by several authors in recent years, using different models and different values of the relevant materials parameters.[10−13,15−18] The consensus among these studies appears to be that this threshold is less than 2%, with values as small as 1.7% reported.[10,17,18]

TABLE 1. Material Parameters Used To Compute the Strain-Dependent Band Gap Energies of Ge

b (eV)	−2.16[10]
a_v (eV)	1.24[11,37]
a_c (eV)	−8.24[11,37]
$\Xi_d + \Xi_u/3$ (eV)	−2.34[11]
$E_{g\Gamma}$ (eV)	0.802[40]
$E_{g\Gamma}$ (eV)	0.661[40]
Δ (eV)	0.290[40]
C_{11} (GPa)	128.53[10]
C_{12} (GPa)	48.26[10]

The use of biaxial tensile strain in other crystallographic planes has also been investigated theoretically.[17,18] These studies suggest that Ge films grown on {110}-oriented substrates can also possibly be made direct-band gap, but only at rather large (probably experimentally unachievable) biaxial strain levels of about 4.5%.[17] In contrast, in {111} Ge, the absolute conduction band minima remain in the L valleys for all realistic tensile strain values. In any case, it should be noted that the {100} orientation, which appears to be most favorable in the present context, is also of particular technological significance, as it is the most widely used crystallographic orientation in microelectronics.

For uniaxial strain, it has been predicted that tension along the ⟨111⟩ direction can produce a direct band gap in Ge, owing to a large nonlinear drop in the conduction band edge at Γ.[14] The corresponding strain threshold has been estimated at 4.2% (other authors have computed a significantly smaller value of 1.05%,[18] which, however, does not appear to be corroborated by any known experimental evidence). In principle,

uniaxial strain may be employed in conjunction with Ge nanowires, whose ultrasmall cross sections may allow for the introduction of particularly high strain levels without plastic deformation. This idea has recently been explored in ref 32, where uniaxial strain values along the ⟨100⟩ direction exceeding 3% were reported, albeit without any claim regarding the formation of direct-band gap Ge. In fact, a theoretical strain threshold of 4.7% was cited in this work.[32]

Valence Bands and Optical Matrix Elements. To quantify the ability of tensile strain in Ge to increase the interband radiative recombination efficiency and to enable the formation of population inversion across the direct energy band gap, it is also important to understand how the valence bands are modified in the presence of strain. In the context of deformation potential theory, a relatively simple model can be constructed from the Luttinger–Kohn Hamiltonian through the addition of a small number of terms proportional to the strain tensor elements.[36] If one considers a 6 × 6 Hamiltonian matrix and again assumes that all off-diagonal strain elements are zero, the band-edge energies of the HH and LH valence bands can be computed as follows

$$E_{\rm HH} = E_{\rm HH}^{(0)} - P_\varepsilon - Q_\varepsilon \quad (4)$$

$$E_{\rm LH} = E_{\rm LH}^{(0)} - P_\varepsilon + \frac{1}{2}\left(Q_\varepsilon - \Delta + \sqrt{\Delta^2 + 2Q_\varepsilon\Delta + 9Q_\varepsilon^2}\right) \quad (5)$$

where

$$P_\varepsilon = -a_{\rm v}(\varepsilon_{xx} + \varepsilon_{yy} + \varepsilon_{zz}) \quad (6)$$

and

$$Q_\varepsilon = -\frac{b}{2}(\varepsilon_{xx} + \varepsilon_{yy} - 2\varepsilon_{zz}) \quad (7)$$

In these equations, $a_{\rm v}$ and b are the hydrostatic and shear deformation potentials of the valence bands, respectively, and Δ is the spin–orbit splitting of unstrained Ge (*i.e.*, the energy separation between the spin–orbit split-off valence band and the degenerate HH and LH bands at Γ).

Figure 2 shows the energies of the conduction and valence band edges of Ge, from eqs 1, 2, 4, and 5, as a function of strain for biaxial tension in a {100} plane, for which eq 3 also applies. The material parameters used in these calculations are listed in Table 1, with all energies referenced to the top of the HH and LH valence bands in the absence of strain. Aside from the aforementioned crossing of the direct and indirect conduction band minima at about 1.9% strain, a large strain-induced splitting of the valence bands at the Γ point is also clearly seen in this figure. Specifically, under tensile strain, the LH band is pushed up in energy relative to the HH one, which implies that interband light emission in this material mostly

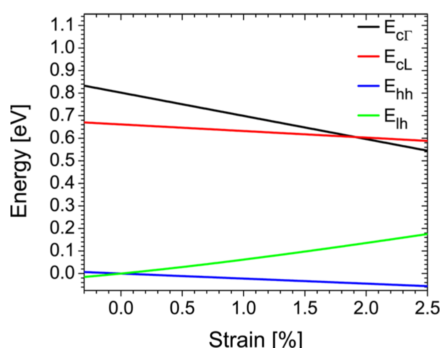

Figure 2. Band-edge energies of the conduction and valence bands of Ge plotted as a function of biaxial strain in a {100} plane. The labels refer to the Γ- and L-conduction band minima and to the LH and HH valence band maxima.

involves recombination of electrons with LHs. At the same time, the direct-band gap energy $E_{g\Gamma} = E_\Gamma - E_{\rm LH}$ monotonically decreases with increasing ε, for example, from its unstrained value of 0.8 eV to 0.46 eV at 2% strain. As a result, emission wavelengths in the short-wave mid-infrared spectral region can be expected in Ge(001) tensilely strained to this degree. This wavelength range has significant technological applications, particularly in the areas of biochemical sensing and spectroscopy.

The dominant role played by the LH valence band in the context of radiative recombination in tensilely strained Ge has two additional important implications. First, the hole density-of-states effective mass is reduced compared to the unstrained case, which is favorable for the purpose of creating a population inversion.[36] In fact, Ge has relatively small effective masses for both the LHs and the Γ-point conduction band electrons compared to the traditional III–V semiconductors used in optoelectronics, something that is a distinct advantage for laser applications. Second, the polarization properties of the emitted light are determined by the symmetry of the LH Bloch functions. To elaborate on this latter point, we consider the momentum matrix elements M of the direct conduction-to-HH (cΓ-HH) and conduction-to-LH (cΓ-LH) transitions for transverse magnetic (TM) and transverse electric (TE) light (defined, respectively, as linearly polarized in the directions perpendicular and parallel to the plane of the biaxially strained layer). The magnitudes squared of these parameters are directly proportional to the probability rates of the respective transitions and can be calculated from the relevant Bloch functions as follows[41]

$$\begin{aligned} |M_{{\rm TM,c}\Gamma\text{-}{\rm HH}}|^2 &= 0 \\ |M_{{\rm TE,c}\Gamma\text{-}{\rm HH}}|^2 &= \frac{3}{2}M_{\rm b}^2 \\ |M_{{\rm TM,c}\Gamma\text{-}{\rm LH}}|^2 &= 3f_z M_{\rm b}^2 \\ |M_{{\rm TE,c}\Gamma\text{-}{\rm LH}}|^2 &= \frac{3}{2}(1 - f_z)M_{\rm b}^2 \end{aligned} \quad (8)$$

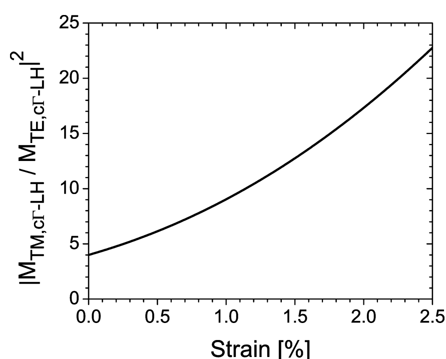

Figure 3. Ratio of the TM- and TE-polarized squared momentum matrix elements associated with cΓ-LH transitions in Ge, plotted as a function of biaxial tensile strain.

where M_b is the bulk momentum matrix element (as defined, *e.g.*, in ref 36) and

$$f_z = \frac{1}{2}\left(1 + \frac{\Delta/3 - 6b\varepsilon}{\sqrt{\Delta^2 - 4b\varepsilon\Delta + 36b^2\varepsilon^2}}\right) \qquad (9)$$

It follows from these equations that cΓ-HH transitions can only emit TE-polarized light, whereas cΓ-LH transitions generally couple to both states of polarization. Furthermore, because f_z is a monotonically increasing function of ε (given that $b < 0$), the latter transitions become increasingly TM-polarized as more and more tensile strain is introduced. To illustrate, in Figure 3, we plot the ratio $|M_{TM,c\Gamma\text{-}LH}/M_{TE,c\Gamma\text{-}LH}|^2$ as a function of ε. The important conclusion is that, in tensilely strained Ge, where interband light emission is dominated by the cΓ-LH transitions, the emitted light is predominantly TM-polarized (*e.g.*, by a factor of 17:1 at 2% strain, based on the plot of Figure 3).

Straining Techniques. In this section, we review approaches to introduce tensile strain in Ge that have been employed. We consider heteroepitaxial growth on suitable templates, use of deposited stressor materials, and the application of stress by mechanical means. Our aim is to provide a perspective of the challenges and opportunities in creating Ge-based group-IV light sources and optoelectronic devices.

Limits on Achievable Strain. In each of these approaches, the amount of strain that can be introduced before a form of irreversible (plastic) structural relaxation occurs is limited. Plastic relaxation, primarily through dislocation formation or through cracking, occurs when the strain energy built up in the material of interest exceeds the thermodynamic and kinetic barriers to make strain relief favorable. The strain energy increases according to the relation[42]

$$dU = \frac{1}{2}\sigma_x\varepsilon_x dV \qquad (10)$$

where U is the strain energy, σ is the normal stress on the material, ε is the corresponding strain, and V is the sample volume. This equation shows two important relationships: (1) For a given film area, the strain energy increases with thickness; and (2) a given strain energy is reached at higher stress for a thinner sheet than for a thicker sheet.

For heteroepitaxial growth, where a thin film is grown on a host substrate having a different lattice constant, in general, the formation of dislocations limits the achievable strain. The mechanics of dislocation formation are well understood.[43] The thermodynamics of strain buildup in growth of lattice-mismatched films and the transition to dislocation formation is expressed through the concept of a critical thickness.[44] The transition to dislocation formation is also dependent on the nature of the substrate. Thus for growth on thin substrates, either supported on a release layer like an oxide or free-standing, the barriers for dislocation formation are lower and the critical thickness for dislocation formation is consequently also lower.[45] Whereas dislocated films can still contain strain, the strain will be laterally nonuniform because of plastic relaxation in the vicinity of dislocations. In terms of tensilely strained Ge, dislocations are undesirable, as they can act as nonradiative recombination sites, limiting the light emission efficiency. Additionally, dislocations can degrade the transport characteristics in electrically injected devices. Laterally nonuniform strain causes in-plane variations of the band structure. Under these conditions, the emission will arise primarily from the high-tensile-strain regions, where the band gap energy is smaller and the density of electrons and holes correspondingly higher. Importantly, this behavior may also mitigate the deleterious effect of dislocations as nonradiative recombination centers, as the relatively higher band gap energy in the immediate surroundings of dislocations may act as a potential energy barrier that limits the number of carriers that can recombine there.

For sheets or ribbons that are mechanically stressed *via* the application of an external tension, the likely mechanism for plastic relaxation is crack formation and fracture. Equation 10 applies for the buildup of strain; except now we have a given volume and the stress is increased until a critical stress is reached. The key quantity is the strain energy release rate, which is defined as the energy dissipated during fracture per unit of newly created fracture surface area. The energy that must be supplied to a crack tip for it to grow must be balanced by the amount of energy required for the formation of new surfaces and for plastic deformation. The energy release rate is given by[46]

$$G \equiv -\frac{\partial(U - W)}{\partial A} \qquad (11)$$

where U is the potential energy available for crack growth (the strain energy in the material), W is the work associated with any external forces present, and A is the crack area (crack length for two-dimensional problems).

A crack will grow when the energy release rate G is greater than or equal to a critical value, G_c, called the

fracture energy, which is a material property independent of the applied loads and the geometry of the body. For a thin sheet, the potential energy U for a fixed value of strain is lower at a lower thickness (see eq 10). Therefore, the energy release rate G reaches the critical value G_c at higher strain levels for a thinner sheet. The effect of cracks on achievable strain is similar to that of dislocations. Around cracks, the material will relax strain, and thus strain nonuniformities result, and the average maximum strain is limited. For tensilely strained Ge, again, light emission will arise primarily from the high-strain regions, where the band gap energy is smaller and the density of electrons and holes correspondingly higher. Cracks will limit the light emission efficiency and degrade the transport characteristics in electrically injected devices.

For the group of techniques that use deposited stressor layers, the high levels of strain required to obtain direct-band gap Ge frequently are not achievable because the stressor layer cannot generate a high enough level of stress for the thickness of the Ge layer used. Thus defect formation may not even be an issue in some of these methods. Thinner Ge layers would be more highly strained (see eq 10) and may be subject to dislocation formation as described above. If stressor layers that bend the Ge sheet are used, the strain varies through the thickness of the sheet and so will the band gap and shape of bands.

Heteroepitaxial Growth. Strain engineering in electronic and optoelectronic device fabrication is generally based on heteroepitaxy. As long as the film thickness is kept below the critical value for plastic deformation, the growth proceeds in a pseudomorphic fashion and the film is strained as it adjusts to the substrate in-plane crystal structure. The tensile strain required to make Ge direct-band gap is, however, significant, and it is no easy matter to (1) find substrates with appropriate lattice constants to serve as templates and (2) grow a sufficiently thick film without the introduction of massive numbers of dislocations, which, of course, relax the strain. Very thin layers of Ge can be grown pseudomorphically on SiGe substrates that are formed *via* compositionally graded deposition of SiGe on Si.[47] This procedure, used routinely for growing tensilely strained Si, results in compressively rather than tensilely strained Ge because Ge has a larger lattice constant than SiGe, and thus this approach does not suit the purpose of creating direct band gap Ge. Tensile strain in Si does not achieve the same end, as the conduction band minima of Si are too far apart in energy and do not move appropriately with strain.[48] In any case, compositionally graded SiGe substrates contain mosaic features (microcrystalline tilts) and strain inhomogeneities, both caused by dislocation formation during the compositional grading, that ultimately create defects in the strained Si or Ge films grown on top of these substrates.[49−51]

A small amount of tensile strain can be induced in Ge if it is grown on Si and allowed to relax plastically (*i.e.*, *via* formation of dislocations) at high growth temperatures (~900 °C) and subsequently cooled, because of the large difference in thermal expansion coefficients between Ge and Si. Annealing at these high temperatures also somewhat reduces the density of dislocations. The maximum tensile strain that can be obtained in this manner is limited to ~0.3%.[52] This amount of strain is nevertheless useful, even with the induced dislocations: in fact, the combination of this approach with highly degenerate n doping to raise the electronic quasi-Fermi level has led to the recent demonstration of an electrically pumped Ge diode laser.[53]

Alternative growth template materials with lattice constant close to but somewhat larger than that of Ge, such as InGaAs[19−21] and GeSn,[22] have also been investigated. For example, a biaxial tensile strain of up to ~0.25% was obtained in Ge grown on a GeSn buffer layer deposited on a Si substrate by chemical vapor deposition, with the Ge strain depending on the buffer thickness and composition.[22] A 0.5% biaxial tensile strain was introduced in Ge grown on an InGaAs template layer on GaAs with In concentration of 9.8%.[20] The Ge room-temperature photoluminescence (PL) red shifts with increasing In concentration of the substrate, consistent with the increase in tensile strain in the Ge film. The classical approach of using a compositionally graded substrate, here InGaAs layers with increasing In concentration deposited on GaAs and annealed at each step to reduce dislocations, produced much higher biaxial tensile strain values in Ge.[19] For a 10 nm thick Ge film pseudomorphically grown on a graded $In_{0.4}Ga_{0.6}As$ substrate, a biaxial tensile strain of 2.33% (as measured *via* X-ray diffraction and Raman spectroscopy) was reported. This value is well above the expected threshold for direct-band gap behavior (1.9%). Note that the Ge film is very thin, as otherwise it would exceed its critical thickness. Nevertheless, this Ge film would be expected to have threading dislocations throughout it, as well as a mosaic (microtilt) structure and lateral strain inhomogeneities, emanating from the substrate (similar to those found in tensilely strained Si epitaxially grown on compositionally graded SiGe substrates).[49] A large increase in the overall PL peak intensity relative to a similar unstrained Ge sample was reported (greater than 20×), but only at cryogenic temperatures and without the large red shift expected from theoretical considerations (*e.g.*, see Figure 2). The authors did not persuasively comment on the lack of a red shift or the rapid extinction of the PL with increasing temperature. The causes may be related to the extended defects in the grown film that one would expect from the compositionally graded substrate that was used.

Use of Stressor Layers. Tensile strain in Ge can also be obtained *via* the use of suitable stressor layers.

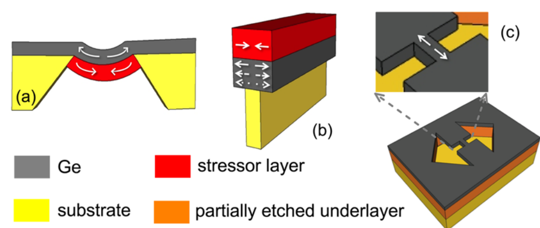

Figure 4. Schematic illustrations of the use of stressor layers to introduce tensile strain in Ge. (a) Cross-sectional image of the geometry used in ref 29 to obtain nominally biaxial tensile strain in an edge-clamped suspended Ge film. (b) Three-dimensional view of the uniaxially strained Ge photonic wires described in ref 28. (c) Uniaxially strained Ge microbridge geometry demonstrated in ref 32. In all figures, the arrows pointing outward (inward) indicate tensile (compressive) strain. The solid, dashed, and dotted arrows in (b) indicate regions of progressively weaker tensile strain.

Illustrative examples are shown in Figure 4. Typically, these layers consist of material under large compressive strain, which is then allowed to relax partially *via* elastic strain sharing with the Ge film. As a result, tensile strain is introduced in the Ge. An example of a suitable geometry that allows for such elastic strain relaxation to take place is illustrated schematically in the cross-sectional image of Figure 4a. This geometry has been demonstrated recently using tungsten (which can be deposited with a compressive stress of approximately 4 GPa) as the stressor layer.[29,54] A 1.6 μm thick Ge film was deposited on a Si substrate and then suspended inside a window by etching away the Si through a patterned layer of SiO_2 on the substrate backside. Because Ge does not grow epitaxially on Si, this film will be highly dislocated. The tungsten stressor layer (up to 900 nm in thickness), deposited on the bottom surface of the edge-clamped suspended Ge film, introduces an average biaxial tensile strain of about 1.1% in the Ge, through a bending of the overall suspended layer. Because the Ge layer is curved, the strain will vary through its thickness, an effect that is not considered. An increase in integrated PL intensity by a factor of approximately 2 was measured, together with a 130 nm red shift in peak emission wavelength.

A similar geometry was employed to strain a layered Ge p-n junction patterned in the shape of a mesa with top-side contacts to the n and p regions, before deposition of the tungsten stressor layer underneath the mesa.[29,54] Strained-Ge photodiodes and light-emitting diodes (LEDs) were fabricated; their responsivity and emission spectra, respectively, could be red-shifted through the deposition of stressor layers of increasing thickness. The LED forward current was also found to increase with increasing tensile strain, a behavior that was attributed to the expected increased intrinsic carrier concentration and enhanced carrier mobility caused by the strain-induced band gap reduction.[7]

Tensilely strained Ge has also been obtained using Si_3N_4 as the stressor material. In the work of ref 28, a compressively strained Si_3N_4 layer was deposited on a highly n-doped Ge film that had been epitaxially grown on GaAs [Ge and GaAs(001) are closely lattice matched, so the Ge was initially unstrained]. When this Si_3N_4 layer, the underlying Ge film, and part of the GaAs substrate are patterned in the shape of a ribbon, as illustrated in Figure 4b, the compressive strain in the Si_3N_4 layer relaxes as its flanks become free to move. Uniaxial tensile strain is correspondingly introduced in the Ge along the direction perpendicular to the long axis of the ribbon. The strain is nonuniform in the direction out of the plane, reaching maximally 0.6% at the Si_3N_4/Ge interface and falling off rapidly with depth into the Ge layer. With this approach, net optical gain was reported for light propagating along the ribbon. Similar to the laser demonstration of ref 53, this measured gain was enabled primarily by degenerate n-doping of the Ge film. As discussed in the following, distinct advantages in terms of creating Ge light sources are obtained with undoped Ge, but substantially larger strain levels are needed to allow for a population inversion in the absence of high n-doping.

In a somewhat different approach,[30] uniaxial tensile strain of approximately 1% in suspended Ge microbridges (ribbons) was obtained, using the deposition of tensilely strained Si_3N_4 stressor layers on both ends of the bridge [Si_3N_4 films can be either compressively or tensilely strained depending on the evaporation conditions]. The same approach was also applied to a cross-shaped bridge to obtain biaxial tensile strain near the cross center. Unexpectedly large PL enhancements (by factors of over 100) were reported with these samples; it is likely, however, that heating of the suspended membranes by the high-power continuous wave pump light used in the PL measurements played a role in these findings.[31]

Highly uniaxially strained Ge layers have been fabricated by taking advantage of the thermal mismatch between Si and Ge, which allows using Si as the stressor material.[32] Ge is grown directly on a Si-on-insulator (SOI) or bulk Si substrate using low-energy plasma-enhanced chemical vapor deposition. After growth, a series of annealing cycles is performed *in situ* to reduce the density of threading dislocations, while at the same time introducing a small amount of biaxial tensile strain in the Ge (about 0.15%). As discussed earlier, this strain is caused by the mismatch between the thermal expansion coefficients of Si and Ge and the resulting hindered relaxation of the Ge layer upon cooling. Constricted Ge structures (in the shape of suspended microbridges, as shown in Figure 4c) are then patterned using electron-beam lithography, dry etching of the Ge layer, and a selective wet etch of the material underneath (either Si or the SOI buried oxide). Because stress is inversely proportional to cross-sectional area, the constricted regions in this geometry experience much larger tensile strain

compared to the rest of the Ge film. In fact, uniaxial strain values up to 3.1% were measured in these regions using Raman microscopy. A 210 meV peak energy shift in the emission with respect to bulk Ge and a strong increase (25×) in the spectrally integrated micro-PL intensity were also observed. No claim of a transition to direct-bandgap Ge was made; in fact, a threshold of 4.7% tensile strain was cited.[32]

Nam *et al.* followed the same concept but used the small (about 0.2%) pre-existing tensile strain in the Ge template layer of a Ge-on-insulator (GOI) substrate.[33] They obtained Ge wires uniaxially strained up to 2.8%. Furthermore, they showed that the strain (and therefore the band gap energy) in the patterned Ge film could be modulated as a function of in-plane position by varying the wire width, effectively producing strain-induced pseudo-heterostructures, which had earlier been demonstrated for Si nanowires.[55] A large enhancement in micro-PL intensity was observed and attributed mostly to carrier confinement in the high-strain regions.

Application of Mechanical Stress. Finally, Ge can be strained through the application of external mechanical stress. In general, this approach is quite flexible and, in fact, historically has provided the first means used to investigate strain engineering of semiconductors.[56] Furthermore, it allows tailoring the material properties after sample preparation (by varying the applied stress), a feature that is attractive for basic studies as well as device applications. Recently, the same general approach has also been applied to nanostructures based on III−V semiconductors, such as GaAs nanowires.[57,58] In the context of Ge, the use of mechanical stress to enable optical gain has been investigated numerically in ref 13. The specific geometry considered in that study consists of a cross-shaped suspended Si platform supporting a Ge disk at its center, in the presence of a vertical force of 330 mN applied at the platform center. This force may be obtained using an L-shape hook in the external chip package or an electrostatic actuator based on micro-electro-mechanical system (MEMS) technology. The resulting stress field distribution, computed by finite element analysis, is shown in Figure 5. At the platform center, where the Ge active layer resides, a maximum biaxial tensile stress of 5 GPa is obtained, corresponding to a strain level of about 2.7%. This geometry should therefore be suitable for the development of direct-band gap Ge light-emitting devices.

At the same time, straining *via* the application of mechanical stress has the important limitation that, when bulk samples are employed, only small amounts of tensile strain can be introduced before the onset of plastic relaxation *via* defect formation. The reason is that the strain energy for a given stress increases with thickness (volume) as discussed earlier (eqs 10 and 11). This limitation is clearly illustrated in the initial attempts

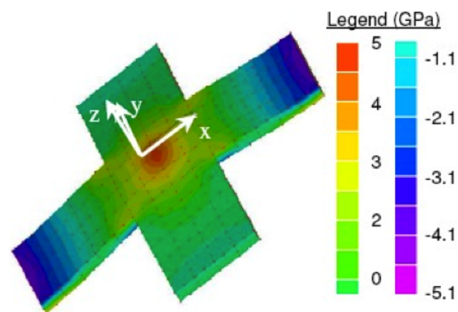

Figure 5. Calculated in-plane stress distribution on a cross-shaped suspended Si platform supporting a Ge disk at its center. Reproduced with permission from ref 13. Copyright 2009 The Optical Society.

to study direct-band gap light emission from mechanically stressed Ge.[23,24] In particular, in the work described in ref 23, a maximum biaxial tensile strain of only 0.6% (limited by sample debonding or fracture; see eq 11) could be introduced in a 28 μm thick Ge film mounted on a bulge/blister test apparatus, leading to a red shift in emission wavelength (by about 125 nm) but no concomitant increase in output intensity. In the work described in ref 24, an n-doped Ge wafer was used, featuring an even smaller fracture limit of less than 0.4% strain, and leading to a small (1.8×) increase in measured PL intensity.

Much larger PL enhancements (almost 100×) were observed using tensilely strained Ge nanocrystals.[27] These samples were fabricated by mortar grinding of undoped (100) bulk Ge wafers, and the lattice constants measured from several electron diffraction patterns suggest a 2.2 ± 1.1% strain. The emission wavelength was not red-shifted compared to unstrained bulk Ge, a result that was attributed to quantum confinement effects.

Mechanically Stressed Nanomembranes. For samples with planar geometries, which are more directly compatible with device applications, nanoscale thicknesses are essential to enable large biaxial strains. Traditionally, single-crystal semiconductor films with thicknesses of only a few tens of nanometers or less have been the exclusive domain of heteroepitaxial systems, but, as already discussed above, such systems have so far not been able to achieve the requisite strains in Ge (or if such strains were nominally achieved, the light emission properties did not support the formation of direct-band gap Ge). The emergence of NM technology has created significant new opportunities for thin-film materials science and applications.[35,48,50,51,59−68] This technology is based on the complete or partial release of a thin semiconductor layer from its original substrate *via* the selective etch of an underlying sacrificial layer. The resulting membranes can be single-crystal while at the same time exhibiting exceptional flexibility, with the capability of folding and unfolding many times without damage.

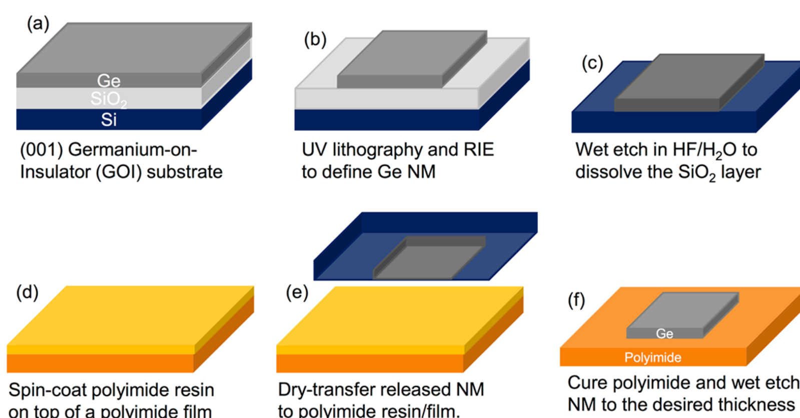

Figure 6. Schematic illustration of the Ge NM fabrication process used in the work of refs 25 and 26.

When completely released from their handle wafer, they can be transferred (using one of several techniques such as wet transfer or dry printing) and strongly adhered onto a variety of host substrates. Because of their extreme geometrical aspect ratios and the resulting unique mechanical properties, NMs offer novel opportunities for strain engineering, both through spontaneous elastic strain sharing in multilayer NMs and through the external application of mechanical stress. For the same reasons, they have been shown to provide an attractive high-performance alternative to organic semiconductors for applications in flexible electronics and optoelectronics. For example, electronic devices can be fabricated on the NMs prior to the release step, followed by transfer onto a new host substrate. This approach is highly desirable, particularly when the new substrate cannot withstand the high-temperature processing necessary for electronic device fabrication, as is the case for most organic materials. By performing the high-temperature processing steps on the NM before release, it is thus possible to make extremely fast flexible electronics, using organic films as host substrates.[60,68]

In recent work,[25,26] a simple straining technique involving the use of air to pressurize a cell covered with a round sheet has been applied to Ge(001) NMs to demonstrate biaxial tensile strain sufficiently large to create a direct-band gap. In order to illustrate the advantages of using NMs to create highly strained Ge for photonic applications, we describe the procedures and results for this approach in somewhat greater detail.

The fabrication process used to strain Ge in this manner is illustrated schematically in Figure 6. Free-standing NMs are first created by releasing the top Ge template layer of a (001)-oriented, low-doped GOI wafer, using a wet etch to dissolve the underlying buried oxide (BOX) layer. To prepare for the fabrication of the NMs, the GOI substrates are cleaned with acetone and isopropyl alcohol and patterned to define the membrane boundaries and etchant access holes. Reactive ion etching (RIE) is employed to etch the Ge template layer along these boundaries, followed by a wet etch in a mixture of 49% hydrofluoric acid and water solution (1/10) to dissolve the underlying SiO_2 layer. The resulting Ge NMs settle onto the original Si host wafer, from which they can be easily removed. The NMs are subsequently transferred and bonded onto 125 μm thick flexible polyimide (PI) films (Kapton, DuPont), by using spin-on liquid PI as a glue layer and pressing the membrane onto the PI film. After transfer, the spun-on PI is cured at 350 °C and the Ge NM is thinned from its original thickness (140−160 ± 5 nm) to the desired thickness, using a wet etch with dilute hydrogen peroxide (H_2O_2).

In order to stretch the NM in a highly controllable isotropic fashion, the PI film is used to seal an otherwise rigid cavity that is then filled with gas whose pressure can be reliably and reproducibly increased. A schematic illustration of the experimental sample mount is shown in Figure 7, together with an optical micrograph of a Ge NM bonded onto a PI film. In this arrangement, the NM lies on the surface of an expanding sphere of PI, so that the resulting strains are biaxial. The spherical expansion of the PI is partially a bending mode, in which maximum tensile strain is created at the top surface, where the NM resides. Because the NM is very thin, the tensile strain throughout its thickness is for all intents a constant, and the strain is biaxial tensile.

This use of very thin NMs and a simple spherical expansion technique allows for the introduction of large values of biaxial strain, limited only by the threshold for plastic deformation or cracking of the Ge NM as described in eqs 10 and 11. The PI substrate in any case may deform plastically, but this deformation does not influence the threshold for the NM and does not influence the reversibility of the strain application in the NM.

The biaxial strain in the plane of the NMs is measured as a function of applied stress (*i.e.*, gas pressure) *via* Raman spectroscopy. Raman spectroscopy is extremely sensitive to strain in Ge, using the Raman line

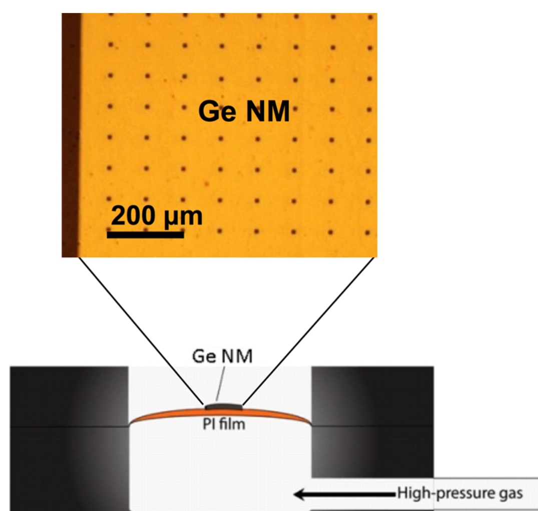

Figure 7. Schematic illustration of the experimental setup used to introduce biaxial tensile strain in Ge NMs. A top-view optical micrograph of a NM bonded onto a PI film is also shown. The periodic black dots are etchant access holes used to expedite the Ge NM release from GOI. Reproduced with permission from 25. Copyright 2011 National Academy of Sciences.

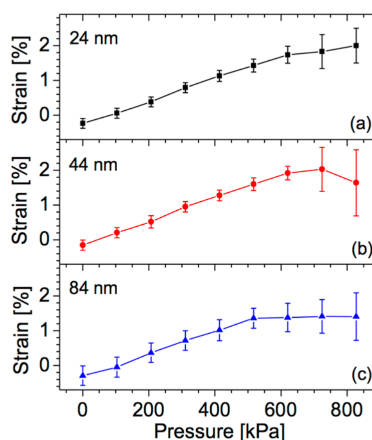

Figure 8. Strain/stress curves measured *via* Raman spectroscopy with three Ge NMs having different thicknesses. A pressure of 800 kPa translates into a biaxial stress of ~2.8 GPa in the NM. The Ge NM after mounting on PI contains a small compressive strain. Reproduced with permission from ref 25. Copyright 2011 National Academy of Sciences.

associated with Ge–Ge stretch vibrations. The shift of this line $\Delta\omega$ can be related to strain ε using $\varepsilon = -B\Delta\omega$, where the coefficient B depends on known values of the Ge deformation potentials.[69] Representative strain results, measured for Ge NMs of different thicknesses, are shown in Figure 8. As the sample mount is pressurized, the measured biaxial tensile strain (averaged over typically 10 random sites on the NM) initially increases linearly with the applied stress, as expected. At sufficiently high stress, and depending on the Ge NM thickness, local strain relaxation occurs in the NM *via* the formation of microcracks. These cracks, visible in the Raman microscope, produce regions of locally lower strain, so that the average over the Raman laser spot size and the random sites measured for each pressure begins to saturate. In this high-stress regime, more and more of the NM area no longer contributes to the maximum strain, leading also to an increase in the standard deviation in the measurements. The results plotted in Figure 8 show that the strain threshold for the formation of cracks increases with decreasing NM thickness, as expected from the earlier discussion of the dependence of strain energy on NM thickness and crack formation (see eqs 10 and 11). Specifically, because the amount of strain energy stored in the NM is directly proportional to its thickness, when very thin compared to the substrate, the NM contains insufficient strain energy to drive defect formation.[42] Average biaxial tensile strain levels of approximately 2% (as needed for the formation of direct-band gap Ge) can be obtained in NMs with thicknesses of about 50 nm or less with the above approach and without any special surface treatment. A more recent thickness-dependent strain analysis of thicker Ge films grown on InGaAs buffer layers demonstrates a similar trend, with the strain relaxation threshold decreasing with increasing film thickness.[21]

Optical Properties of Tensilely Strained Ge Nanomembranes. In this section, we describe the radiative properties of Ge under the extreme tensile strain conditions enabled by NM straining technology. Recent experimental demonstrations of strain-enhanced light emission and the formation of population inversion under optical pumping are reviewed and compared to numerical calculations showing that tensilely strained Ge NMs can provide substantial optical gain under realistic pumping conditions. These results are quite general and apply to other potential straining methods that can provide sufficiently high strain.

Optical Gain Calculations. The optical gain spectrum of tensilely strained Ge associated with electronic transitions between the direct conduction band minimum and the HH or LH valence bands can be calculated as follows[70]

$$g(h\nu_0) = \frac{C}{h\nu_0}\int |M_{\mathrm{TM,TE}}(E_{21})|^2 \rho_r(E_{21})[f_2 - f_1]\xi(h\nu_0 - E_{21})\mathrm{d}E_{21} \quad (12)$$

In this expression, g is the gain coefficient (which describes the variation in optical intensity I with propagation distance z according to the equation $\mathrm{d}I/\mathrm{d}z = gI$), ν_0 is the optical frequency, $M_{\mathrm{TM,TE}}$ is the polarization-dependent momentum matrix element given by eq 8 for both cΓ-LH and cΓ-HH transitions, $\rho_r(E_{21})$ is the reduced density of states, f_1 and f_2 are the occupation probabilities of, respectively, the valence band and conduction band states having energy difference E_{21} and equal wave vector, and $\xi(h\nu_0 - E_{21})$ is the line shape function that describes gain broadening. Finally,

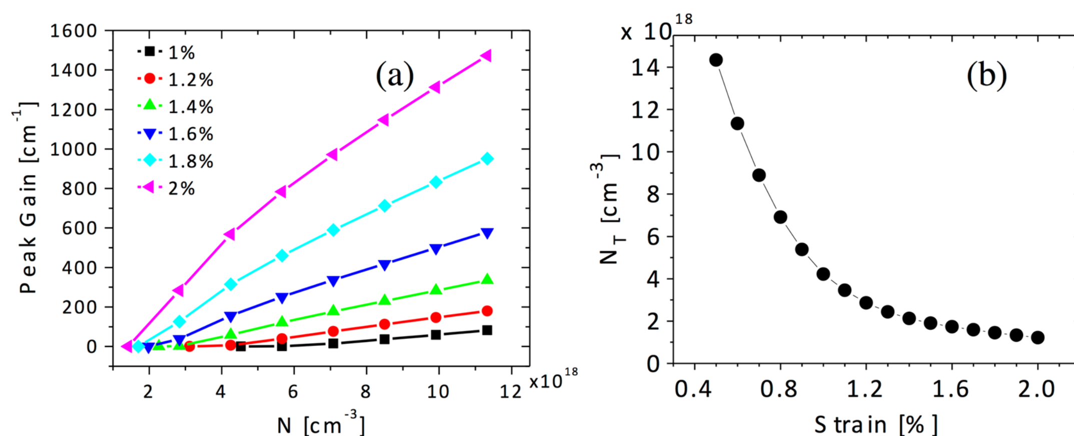

Figure 9. Calculated optical gain properties of tensilely strained Ge. (a) Peak TM gain coefficient plotted as a function of carrier density for different strain values. (b) Transparency carrier density plotted as a function of strain. From ref 26. Copyright 2013 Wiley.

the constant C is given by $C = q^2h/2n\varepsilon_0 cm_0^2$, where n is the refractive index, q the electron charge, h Planck's constant, ε_0 the permittivity of free space, c the speed of light in vacuum, and m_0 the electron mass. Parabolic energy bands are assumed in these calculations, so that the expression in eq 12 only depends on a few well-established material parameters, namely, the band gap energies, the effective masses, and the momentum matrix elements, which can be computed as a function of strain using data from the literature.[26]

As explained above, radiative recombination in tensilely strained Ge NMs predominantly involves direct transitions into the LH valence band, which mostly produce TM-polarized light propagating along the plane of the NM. In Figure 9a, we show the calculated peak gain coefficient provided by these cΓ-LH transitions for TM radiation, plotted as a function of injected carrier density for different values of the applied tensile strain. Undoped Ge and room-temperature emission are assumed in these calculations. At the lowest strain considered in the figure (1 %), no appreciable gain is obtained even under extremely high pumping conditions (*i.e.*, for $N > 10^{19}$ cm^{-3}). As the strain is increased above approximately 1.4%, peak gain values of several 100 cm^{-1} are obtained with lower and lower densities of injected carriers (similar and even larger values have been predicted in more recent calculations[71]). In the same strain regime, transparency carrier densities N_t on the order of a few 10^{18} cm^{-3} are computed, as illustrated in Figure 9b, where N_t is plotted as a function of ε. It should be noted that these values of peak gain coefficient and transparency carrier density are comparable to those of traditional optical gain media based on III–V semiconductors.[36,70] The important conclusion is that tensilely strained Ge NMs are similarly well-suited to the development of diode lasers.

Photoluminescence Measurements. Strained-Ge NM light emission properties have been investigated on undoped membranes having thicknesses between 24 and 100 nm *via* room-temperature PL measurements,[25,26] using a low-duty-cycle pulsed pump source to avoid any appreciable sample heating. To clarify in detail the connection between light emission and strain-dependent band structure, and to illustrate the factors that must be taken into consideration, this section frames the discussion in terms of a specific case, a 40 nm thick Ge NM strained to different degrees. The measurements show a significant red shift in emission wavelength and enhancement in PL intensity with increasing tensile strain. This behavior is consistent with the strain-induced lowering of the Γ-point conduction band edge relative to the L valley minima described earlier, so that at high strain more and more of the photoexcited electrons thermalize near the Γ minimum, where they can efficiently recombine *via* interband light emission. The data measured for the 40 nm thick membrane up to a maximum strain of 1.78% are shown in Figure 10a.

In order to compare these PL data with theoretical expectations, the measured spectra were numerically fitted with multiple Gaussian curves. The resulting peak emission energies are plotted *versus* strain in Figure 10b (symbols); they are found to be in good agreement with the calculated direct and indirect conduction-to-heavy-hole and conduction-to-light-hole band gap energies (solid lines). This comparison between experimental and theoretical emission energies also shows that in all spectra of Figure 10a the main peak is due to cΓ-HH transitions, even though under tensile strain the LH band resides at higher energy and therefore has higher hole occupancy, compared to the HH band (*e.g.*, see Figure 1b). This behavior is a result of the aforementioned polarization selection rules: cΓ-LH transitions mostly generate TM-polarized photons that propagate on the plane of the NM and therefore cannot be detected in standard surface emission PL measurements. For the same reason, the full increase in light emission efficiency brought about by the strain-induced band gap modifications cannot be fully quantified based on the data of Figure 10a.

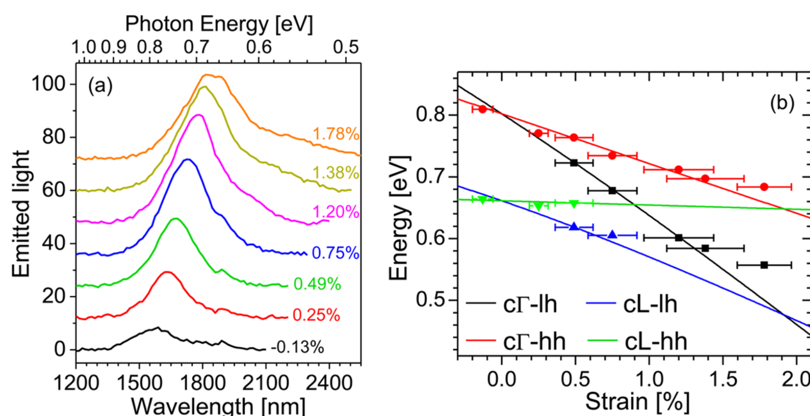

Figure 10. Light emission properties of a tensilely strained 40 nm thick Ge NM. (a) Room-temperature PL spectra of this NM for different strain values. (b) Symbols: peak emission energies obtained from the spectra of (a), plotted as a function of strain. Lines: calculated band gap energies between the Γ- or L-conduction band minima and the HH or LH valence band maxima. Reproduced with permission from ref 25. Copyright 2011 National Academy of Sciences.

At the highest measured strain in this figure, the cΓ-HH and cΓ-LH contributions to the PL spectrum can be clearly resolved, offering a unique opportunity to estimate the quasi-equilibrium carrier density N produced by the pump pulses, and therefore to ascertain whether the NM may already be pumped above transparency.[25,26] The theoretical model described previously can be used to calculate the TE-polarized spontaneous emission spectrum due to both cΓ-HH and cΓ-LH transitions. With the assumption of perfectly parabolic energy bands, the only fitting parameter (besides an overall multiplicative factor) is N, which depends uniquely on the relative height of the experimental cΓ-HH and cΓ-LH emission peaks. The results of this analysis are shown in Figure 11, where the symbols represent the PL data from Figure 10a at 1.78% tensile strain (now normalized to the spectral response of the detection system and plotted *versus* photon energy); the dashed lines are the Gaussian fits used to infer the emission energies, and the solid line is the theoretical fit to the calculated spontaneous emission spectrum. The agreement with the data is quite good, except for the dip between the two peaks in the theoretical spectrum, which has been ascribed to the assumption of parabolic bands.[25,26] From this analysis, a carrier density $N = 3.9 \times 10^{18}$ cm^{-3} was inferred,[26] well above the calculated transparency value at the same strain level (1.5×10^{18} cm^{-3} as shown in Figure 9b). The corresponding theoretical gain spectrum, as computed with eq 12, is shown in the inset, where a large peak value of 250 cm^{-1} (at a wavelength of about 2.3 μm) is observed. Therefore, the analysis of Figure 11 suggests that if the same strained NM were placed in an optical cavity for in-plane propagating light, with reasonably low losses and high optical confinement, lasing action would be feasible.

In ref 25, light emission from a thinner (24 nm) NM under 2% tensile strain, beyond the expected threshold for the formation of direct-band gap Ge, was also

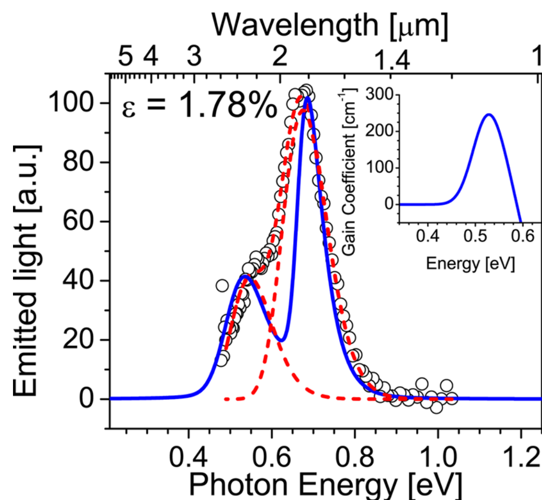

Figure 11. Normalized PL spectrum of the 40 nm thick Ge NM of Figure 10 at a strain of 1.78% (symbols) and calculated TE-polarized spontaneous emission spectrum (solid line). The dashed lines are Gaussian fits to the experimental data. The inset shows the calculated TM gain spectrum of Ge at the same strain level and carrier concentration inferred from this analysis. From ref 26. Copyright 2013 Wiley.

reported. The corresponding spectrum was consistent with the calculated cΓ-HH transition energy under such strain conditions. However, the overall luminescence intensity of this ultrathin sample was found to be relatively weak, likely because of reduced absorption of the pump light and increased nonradiative surface recombination, which prevents the detailed analysis described above.

Stronger emission from tensilely strained Ge at the threshold of direct-band gap behavior has been obtained more recently using a 30 nm thick NM coated with a periodic array of amorphous Ge pillars.[72] A scanning electron microscopy (SEM) image and a schematic cross-sectional view of this sample are shown in Figure 12a. The grating allows outcoupling the in-plane emitted light *via* first-order diffraction in

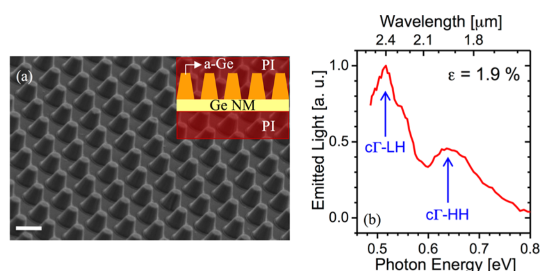

Figure 12. (a) SEM image of a periodic array of amorphous Ge (a-Ge) pillars fabricated on a Ge NM on PI. The scale bar is 1 μm. Inset: schematic cross-sectional view of the same sample. (b) Normalized PL spectrum of a similar sample under 1.9% tensile strain. Reproduced with permission from ref 72. Copyright 2013 American Institute of Physics.

the direction perpendicular to the NM, leading to substantially enhanced PL intensity, particularly at high strain when most of the NM luminescence is TM-polarized. To illustrate, the normalized PL spectrum of this sample at 1.9% strain is shown in Figure 12b. In contrast to bare NMs (*e.g.*, as in Figure 10a), this spectrum is dominated by the long-wavelength cΓ-LH transitions, consistent with the higher density of LHs compared to HHs under tensile strain. With the same sample, a large strain-induced PL efficiency enhancement of >11× was also reported.[72]

CONCLUSIONS AND OUTLOOK

We have reviewed recent work aimed at introducing large tensile strain in Ge for the purpose of significantly modifying its radiative properties, because Ge fundamentally changes the nature of its band structure under tensile strain. Although considerable effort has been devoted to achieving high tensile strain in Ge using heteroepitaxy, a lack of optimally suited growth templates has resulted in innovative ideas but limited success. More recent work has involved the use of mechanically stretched thin sheets or ribbons of Ge, either *via* strain sharing with a stressor layer or through the application of an external force. In particular, the latter approach, applied to ultrathin single-crystal Ge NMs, has enabled the measurement of pronounced luminescence spectra at strain levels close to or beyond the threshold where Ge becomes a direct-band gap semiconductor. A detailed analysis of these results suggests the presence of population inversion under realistic pumping conditions, consistent with theoretical expectations.

Ultrathin membranes under large biaxial tensile strain therefore represent a very promising material platform for the development of infrared optoelectronic devices based on Ge, including lasers. Importantly, such lasers could be developed without the need for degenerate n-doping, as necessitated in prior work,[53] and thus they would not suffer from the large free-carrier absorption losses and fast nonradiative Auger recombination that are byproducts of high doping. In this context, the key remaining challenge is the development of a laser cavity that can provide strong optical confinement and feedback in a NM with highly subwavelength thickness. Photonic crystal cavities consisting of dielectric pillars directly fabricated on the NMs, such as the structure shown in Figure 12a, can provide an optically thick layer for the confinement of the in-plane-propagating emitted light, while at the same time preserving the NM flexibility.

An additional challenge is the development of electrically injected devices. This issue can be addressed with the fabrication of lateral p-(i)-n junctions in the active NM *via* ion implantation and surface passivation, an approach that has already been demonstrated for the development of flexible (unstrained) Ge NM photodiodes.[63]

A third challenge is to extend the amount of strain that can be introduced into the NM without the formation of defects. Defects and cracks typically initiate at stress concentration points. Research into adsorbed layers of agents that increase the barrier for the initiation of defects offers a large new opportunity involving the combination of expertise in surface science and mechanics. So far, very little attention has been focused on this materials science issue. The use of adsorbed layers for surface passivation may also reduce any potential effect of surface recombination on radiative efficiency,[73] and therefore, its investigation in the context of strained-Ge nanostructures represents another important area of future work.

From the strain dependence of the Ge direct-band gap energy (Figure 2), one expects that the emission wavelength of tensilely strained Ge lasers could be tuned across the 2.1−2.5 μm mid-infrared atmospheric transmission window. This spectral region is technologically important for use in biochemical sensing and spectroscopy, where the distinctive absorption features of many molecular species can be exploited for their sensitive detection and potential identification. Specific applications include environmental monitoring, bioagent detection for security screening, medical diagnostics (*e.g.*, *via* breath analysis), and industrial process control. It should be noted that the 2.1−2.5 μm spectrum lies at the boundary of what is presently covered by mature semiconductor laser technologies, such as GaAs- and InP-based diode lasers on the short-wavelength side and III−V quantum cascade lasers at longer wavelengths.[74] Thus, sufficiently tensilely strained Ge is also attractive for the purpose of extending the overall spectral reach of mid-infrared optoelectronics.

Conflict of Interest: The authors declare no competing financial interest.

Acknowledgment. The preparation of this review was supported by the National Science Foundation under Grant No. DMR-0907296 (C.B. and R.P.) and by the Department of Energy

under Grant No. DE-FG02-03ER46028 (J.R.S.P., F.C., and M.G.L.). Work described in this review that was performed at BU and UW was supported by these same grants. Support for growth and Raman spectroscopy facilities at UW was provided by DOE Grant No. DE-FG02-03ER46028.

REFERENCES AND NOTES

1. Chui, C. O.; Saraswat, K. C. Advanced Germanium MOS Devices. In *Germanium-Based Technologies: from Materials to Devices*; Claeys, C., Simoen, E., Eds.; Elsevier: Amsterdam, 2007; pp 363−386.
2. Michel, J.; Liu, J.; Kimerling, L. C. High-Performance Ge-on-Si Photodetectors. *Nat. Photonics* **2010**, *4*, 527–534.
3. Boucaud, P.; El Kurdi, M.; Ghrib, A.; Prost, M.; de Kersauson, M.; Sauvage, S.; Aniel, F.; Checoury, X.; Beaudoin, G.; Largeau, L.; Sagnes, I.; Ndong, G.; Chaigneau, M.; Ossikovski, R. Recent Advances in Germanium Emission. *Photonics Res.* **2013**, *1*, 102.
4. Liu, J.; Kimerling, L. C.; Michel, J. Monolithic Ge-on-Si Lasers for Large-Scale Electronic-Photonic Integration. *Semicond. Sci. Technol.* **2012**, *27*, 094006.
5. Posthuma, N. E.; Van der Heide, J.; Flamand, G.; Poortmans, J. Emitter Formation and Contact Realization by Diffusion for Germanium Photovoltaic Devices. *IEEE Trans. Electron Devices* **2007**, *54*, 1210–1215.
6. Lee, M. L.; Fitzgerald, E. A.; Bulsara, M. T.; Currie, M. T.; Lochtefeld, A. Strained Si, SiGe, and Ge Channels for High-Mobility Metal-Oxide-Semiconductor Field-Effect Transistors. *J. Appl. Phys.* **2005**, *97*, 011101.
7. Chu, M.; Sun, Y. K.; Aghoram, U.; Thompson, S. E. Strain: A Solution for Higher Carrier Mobility in Nanoscale MOSFETs. *Annu. Rev. Mater. Res.* **2009**, *39*, 203–229.
8. Soref, R. A.; Friedman, L. Direct-Gap Ge/GeSn/Si and GeSn/Ge/Si Heterostructures. *Superlattices Microstruct.* **1993**, *14*, 189–193.
9. Liang, D.; Bowers, J. E. Recent Progress in Lasers on Silicon. *Nat. Photonics* **2010**, *4*, 511–517.
10. Fischetti, M. V.; Laux, S. E. Band Structure, Deformation Potentials, and Carrier Mobility in Strained Si, Ge, and SiGe Alloys. *J. Appl. Phys.* **1996**, *80*, 2234–2252.
11. Menéndez, J.; Kouvetakis, J. Type-I Ge/$Ge_{1-x-y}Si_xSn_y$ Strained-Layer Heterostructures with a Direct Ge Bandgap. *Appl. Phys. Lett.* **2004**, *85*, 1175–1177.
12. Liu, J.; Sun, X.; Pan, D.; Wang, X.; Kimerling, L. C.; Koch, T. L.; Michel, J. Tensile-Strained, n-Type Ge as a Gain Medium for Monolithic Laser Integration on Si. *Opt. Express* **2007**, *15*, 11272–11277.
13. Lim, P. H.; Park, S.; Ishikawa, Y.; Wada, K. Enhanced Direct Bandgap Emission in Germanium by Micromechanical Strain Engineering. *Opt. Express* **2009**, *17*, 16358–16365.
14. Zhang, F.; Crespi, V. H.; Zhang, P. Prediction that Uniaxial Tension along ⟨111⟩ Produces a Direct Band Gap in Germanium. *Phys. Rev. Lett.* **2009**, *102*, 156401.
15. El Kurdi, M.; Fishman, G.; Sauvage, S.; Boucaud, J. Band Structure and Optical Gain of Tensile-Strained Germanium Based on a 30 Band $\mathbf{k}\cdot\mathbf{p}$ Formalism. *J. Appl. Phys.* **2010**, *107*, 013710.
16. Pizzi, G.; Virgilio, M.; Grosso, G. Tight-Binding Calculation of Optical Gain in Tensile Strained [001]-Ge/SiGe Quantum Wells. *Nanotechnology* **2010**, *21*, 055202.
17. Aldaghri, O.; Ikonić, Z.; Kelsall, R. W. Optimum Strain Configurations for Carrier Injection in Near Infrared Ge Lasers. *J. Appl. Phys.* **2012**, *111*, 053106.
18. Tahini, H.; Chroneos, A.; Grimes, R. W.; Schwingenschlögl, U.; Dimoulas, A. Strain-Induced Changes to the Electronic Structure of Germanium. *J. Phys.: Condens. Matter* **2012**, *24*, 195802.
19. Huo, Y.; Lin, H.; Chen, R.; Makarova, M.; Rong, Y.; Li, M.; Kamins, T. I.; Vuckovic, J.; Harris, J. S. Strong Enhancement of Direct Transition Photoluminescence with Highly Tensile-Strained Ge Grown by Molecular Beam Epitaxy. *Appl. Phys. Lett.* **2011**, *98*, 011111.
20. Jakomin, R.; de Kersauson, M.; El Kurdi, M.; Largeau, L.; Mauguin, O.; Beaudoin, G.; Sauvage, S.; Ossikovski, R.; Ndong, G.; Chaigneau, M.; Sagnes, I.; Boucaud, P. High Quality Tensile-Strained n-Doped Germanium Thin Films Grown on InGaAs Buffer Layers by Metal-Organic Chemical Vapor Deposition. *Appl. Phys. Lett.* **2011**, *98*, 091901.
21. de Kersauson, M.; Prost, M.; Ghrib, A.; El Kurdi, M.; Sauvage, S.; Beaudoin, G.; Largeau, L.; Mauguin, O.; Jakomin, R.; Sagnes, I.; Ndong, G.; Chaigneau, M.; Ossikovski, R.; Boucaud, P. Effect of Increasing Thickness on Tensile-Strained Germanium Grown on InGaAs Buffer Layers. *J. Appl. Phys.* **2013**, *113*, 183508.
22. Fang, Y. Y.; Tolle, J.; Roucka, R.; Chizmeshya, A. V. G.; Kouvetakis, J.; D'Costa, V. R.; Menéndez, J. Perfectly Tetragonal, Tensile-Strained Ge on $Ge_{1-y}Sn_y$ Buffered Si(100). *Appl. Phys. Lett.* **2007**, *90*, 061915.
23. El Kurdi, M.; Bertin, H.; Martincic, E.; de Kersauson, M.; Fishman, G.; Sauvage, S.; Bosseboeuf, A.; Boucaud, P. Control of Direct Band Gap Emission of Bulk Germanium by Mechanical Tensile Strain. *Appl. Phys. Lett.* **2010**, *96*, 041909.
24. Cheng, T. H.; Peng, K. L.; Ko, C. Y.; Chen, C. Y.; Lan, H. S.; Wu, Y. R.; Liu, C. W.; Tseng, H. H. Strain-Enhanced Photoluminescence from Ge Direct Transition. *Appl. Phys. Lett.* **2010**, *96*, 211108.
25. Sánchez-Pérez, J. R.; Boztug, C.; Chen, F.; Sudradjat, F. F.; Paskiewicz, D. M.; Jacobson, R. B.; Lagally, M. G.; Paiella, R. Direct-Bandgap Light-Emitting Germanium in Tensilely Strained Nanomembranes. *Proc. Natl. Acad. Sci. U.S.A.* **2011**, *108*, 18893–18898.
26. Boztug, C.; Sánchez-Pérez, J. R.; Sudradjat, F. F.; Jacobson, R. B.; Paskiewicz, D. M.; Lagally, M. G.; Paiella, R. Tensilely Strained Germanium Nanomembranes as Infrared Optical Gain Media. *Small* **2013**, *9*, 622–630.
27. Nataraj, L.; Xu, F.; Cloutier, S. G. Direct-Bandgap Luminescence at Room-Temperature from Highly Strained Germanium Nanocrystals. *Opt. Express* **2010**, *18*, 7085–7091.
28. de Kersauson, M.; El Kurdi, M.; David, S.; Checoury, X.; Fishman, G.; Sauvage, S.; Jacomin, R.; Beaudoin, G.; Sagnes, I.; Boucaud, P. Optical Gain in Single Tensile-Strained Germanium Photonic Wire. *Opt. Express* **2011**, *19*, 17925–17934.
29. Nam, D.; Sukhdeo, D.; Roy, A.; Balram, K.; Cheng, S.; Huang, K.; Yuan, Z.; Brongersma, M.; Nishi, Y.; Miller, D.; Saraswat, K. Strained Germanium Thin Film Membrane on Silicon Substrate for Optoelectronics. *Opt. Express* **2011**, *19*, 25866–25872.
30. Jain, J. R.; Hryciw, A.; Baer, T. M.; Miller, D. A. B.; Brongersma, M. L.; Howe, R. T. A Micromachining-Based Technology for Enhancing Germanium Light Emission *via* Tensile Strain. *Nat. Photonics* **2012**, *6*, 398–405.
31. Boucaud, P.; El Kurdi, M.; Sauvage, S.; de Kersauson, M.; Ghrib, A.; Checoury, X. Light Emission from Strained Germanium. *Nat. Photonics* **2013**, *7*, 162.
32. Süess, M. J.; Geiger, R.; Minamisawa, R. A.; Schiefler, G.; Frigerio, J.; Chrastina, D.; Isella, G.; Spolenak, R.; Faist, J.; Sigg, H. Analysis of Enhanced Light Emission from Highly Strained Germanium Microbridges. *Nat. Photonics* **2013**, *7*, 466–472.
33. Nam, D.; Sukhdeo, D. S.; Kang, J. H.; Petykiewicz, J.; Lee, J. H.; Jung, W. S.; Vuckovic, J.; Brongersma, M. L.; Saraswat, K. C. Strain-Induced Pseudoheterostructure Nanowires Confining Carriers at Room Temperature with Nanoscale-Tunable Band Profiles. *Nano Lett.* **2013**, *13*, 3118–3123.
34. Capellini, G.; Kozlowski, G.; Yamamoto, Y.; Lisker, M.; Wenger, C.; Niu, G.; Zaumseil, P.; Tillack, B.; Ghrib, A.; de Kersauson, M.; El Kurdi, M.; Boucaud, P.; Schroeder, T. Strain Analysis in SiN/Ge Microstructures Obtained *via* Si-Complementary Metal Oxide Semiconductor Compatible Approach. *J. Appl. Phys.* **2013**, *113*, 013513.
35. Scott, S. A.; Lagally, M. G. Elastically Strain-Sharing Nanomembranes: Flexible and Transferable Strained Silicon and Silicon-Germanium Alloys. *J. Phys. D: Appl. Phys.* **2007**, *40*, R75–R92.
36. Chuang, S. L. *Physics of Photonic Devices*; Wiley: Hoboken, NJ, 2009.
37. Van de Walle, C. G. Band Lineups and Deformation Potentials in the Model-Solid Theory. *Phys. Rev. B* **1989**, *39*, 1871–1883.

38. Goni, A. R.; Syassen, K.; Cardona, M. Direct-Band-Gap Absorption in Germanium under Pressure. *Phys. Rev. B* **1989**, *39*, 12921–12924.
39. Ahmad, C. N.; Adams, A. R. Electron Transport and Pressure Coefficients Associated with the L_{1C} and Δ_{1C} Minima of Germanium. *Phys. Rev. B* **1986**, *34*, 2319–2328.
40. www.ioffe.rssi.ru/SVA/NSM/Semicond.
41. Jones, G.; O'Reilly, E. P. Improved Performance of Long-Wavelength Strained Bulk-like Semiconductor Lasers. *IEEE J. Quantum Electron.* **1993**, *29*, 1344–1354.
42. Freund, L. B.; Suresh, S. *Thin Film Materials: Stress, Defect Formation and Surface Evolution*; Cambridge University Press: Cambridge, UK, 2003.
43. Hirth, J. P.; Lothe, J.*Theory of Dislocations*, 2nd ed.; Wiley-Interscience: New York, 1982.
44. Matthews, J. W.; Blakeslee, A. E. Defects in Epitaxial Multilayers: I. Misfit Dislocations. *J. Cryst. Growth* **1974**, *27*, 118–125.
45. Euaruksakul, C.; Kelly, M. M.; Yang, B.; Savage, D. E.; Celler, G. K.; Lagally, M. G. Heteroepitaxial Growth on Thin Sheets and Bulk Material: Exploring Differences in Strain Relaxation *via* Low-Energy Electron Microscopy. *J. Phys. D: Appl. Phys.* **2014**, *47*, 025305.
46. Griffith, A. A. The Phenomena of Rupture and Flow in Solids. *Philos. Trans. R. Soc. London, Ser. A* **1920**, *221*, 163–198.
47. Currie, M. T.; Samavedam, S. B.; Langdo, T. A.; Leitz, C. W.; Fitzgerald, E. A. Controlling Threading Dislocation Densities in Ge on Si Using Graded SiGe Layers and Chemical-Mechanical Polishing. *Appl. Phys. Lett.* **1998**, *72*, 1718–1720.
48. Euaruksakul, C.; Li, Z. W.; Zheng, F.; Himpsel, F. J.; Ritz, C. S.; Tanto, B.; Savage, D. E.; Liu, X. S.; Lagally, M. G. Influence of Strain on the Conduction Band Structure of Strained Silicon Nanomembranes. *Phys. Rev. Lett.* **2008**, *101*, 147403.
49. Mooney, P. M.; Jordan-Sweet, J. L.; Noyan, I. C.; Kaldor, S. K.; Wang, P. C. Observation of Local Tilted Regions in Strain-Relaxed SiGe/Si Buffer Layers Using X-ray Microdiffraction. *Appl. Phys. Lett.* **1999**, *74*, 726–728.
50. Paskiewicz, D. M.; Tanto, B.; Savage, D. E.; Lagally, M. G. Defect-Free Single-Crystal SiGe: A New Material from Nanomembrane Strain Engineering. *ACS Nano* **2011**, *5*, 5814–5822.
51. Evans, P. G.; Savage, D. E.; Simmons, C. B.; Lagally, M. G.; Coppersmith, S. N.; Eriksson, M. A.; Schulli, T. U. Nanoscale Distortions of Si Quantum Wells in Si/SiGe Quantum-Electronic Heterostructures. *Adv. Mater.* **2012**, *24*, 5217–5221.
52. Cannon, D. D.; Liu, J.; Ishikawa, Y.; Wada, K.; Danielson, D. T.; Jongthammanurak, S.; Michel, J.; Kimerling, L. C. Tensile Strained Epitaxial Ge Films on Si(100) Substrates with Potential Application in L-Band Telecommunications. *Appl. Phys. Lett.* **2004**, *84*, 906–908.
53. Camacho-Aguilera, R. E.; Cai, Y.; Patel, N.; Bessette, J. T.; Romagnoli, M.; Kimerling, L. C.; Michel, J. An Electrically Pumped Germanium Laser. *Opt. Express* **2012**, *20*, 11316–11302.
54. Nam, D.; Sukhdeo, D.; Cheng, S. L.; Roy, A.; Huang, K. C. Y.; Brongersma, M.; Nishi, Y.; Saraswat, K. Electroluminescence from Strained Germanium Membranes and Implications for an Efficient Si-Compatible Laser. *Appl. Phys. Lett.* **2012**, *100*, 131112.
55. Huang, M.; Ritz, C. S.; Novakovic, B.; Yu, D.; Zhang, Y.; Flack, F.; Savage, D. E.; Evans, P. G.; Knezevic, I.; Liu, F.; Lagally, M. G. Mechano-Electronic Superlattices in Silicon Nanoribbons. *ACS Nano* **2009**, *3*, 721–727.
56. Jayaraman, A. Diamond Anvil Cell and High-Pressure Physical Investigations. *Rev. Mod. Phys.* **1983**, *55*, 65–108.
57. Zardo, I.; Yazji, S.; Marini, C.; Uccelli, E.; Fontcuberta i Morral, A.; Abstreiter, G.; Postorino, P. Pressure Tuning of the Optical Properties of GaAs Nanowires. *ACS Nano* **2012**, *6*, 3284–3291.
58. Signorello, G.; Karg, S.; Björk, M. T.; Gotsmann, B.; Riel, H. Tuning the Light Emission from GaAs Nanowires over 290 meV with Uniaxial Strain. *Nano Lett.* **2013**, *13*, 917–924.
59. Roberts, M. M.; Klein, L. J.; Savage, D. E.; Slinker, K. A.; Friesen, M.; Celler, G.; Eriksson, M. A.; Lagally, M. G. Elastically Relaxed Free-Standing Strained-Silicon Nanomembranes. *Nat. Mater.* **2006**, *5*, 388–393.
60. Yuan, H. C.; Ma, Z. Q.; Roberts, M. M.; Savage, D. E.; Lagally, M. G. High-Speed Strained-Single-Crystal-Silicon Thin-Film Transistors on Flexible Polymers. *J. Appl. Phys.* **2006**, *100*, 013708.
61. Rogers, J. A.; Lagally, M. G.; Nuzzo, R. G. Synthesis, Assembly and Applications of Semiconductor Nanomembranes. *Nature* **2011**, *477*, 45–53.
62. Kim, D. H.; Ahn, J. H.; Choi, W. M.; Kim, H. S.; Kim, T. H.; Song, J. Z.; Huang, Y. G.; Liu, Z. J.; Lu, C.; Rogers, J. A. Stretchable and Foldable Silicon Integrated Circuits. *Science* **2008**, *320*, 507–511.
63. Yuan, H. C.; Shin, J. H.; Qin, G. X.; Sun, L.; Bhattacharya, P.; Lagally, M. G.; Celler, G. K.; Ma, Z. Flexible Photodetectors on Plastic Substrates by Use of Printing Transferred Single-Crystal Germanium Membranes. *Appl. Phys. Lett.* **2009**, *94*, 013102.
64. Yang, W.; Yang, H.; Qin, G.; Ma, Z.; Berggren, J.; Hammar, M.; Soref, R.; Zhou, W. Large-Area InP-Based Crystalline Nanomembrane Flexible Photodetectors. *Appl. Phys. Lett.* **2010**, *96*, 121107.
65. Park, S.-I.; Le, A.-P.; Wu, J.; Huang, Y.; Li, X.; Rogers, J. A. Light Emission Characteristics and Mechanics of Foldable Inorganic Light-Emitting Diodes. *Adv. Mater.* **2010**, *22*, 3062–3066.
66. Feng, P.; Moench, I.; Huang, G. S.; Harazim, S.; Smith, E. J.; Mei, Y. F.; Schmidt, O. G. Local-Illuminated Ultrathin Silicon Nanomembranes with Photovoltaic Effect and Negative Transconductance. *Adv. Mater.* **2010**, *22*, 3667–3671.
67. Sookchoo, P.; Sudradjat, F. F.; Kiefer, A. M.; Durmaz, H.; Paiella, R.; Lagally, M. G. Strain Engineered SiGe Multiple-Quantum-Well Nanomembranes for Far-Infrared Intersubband Device Applications. *ACS Nano* **2013**, *7*, 2326–2334.
68. Zhou, H.; Seo, J. H.; Paskiewicz, D. M.; Zhu, Y.; Voyles, P.; Zhou, W.; Lagally, M. G.; Ma, Z. Q. Fast Flexible Electronics with Strained Silicon Nanomembranes. *Sci. Rep.* **2013**, *3*, 01291.
69. Cerdeira, F.; Buchenauer, C. J.; Cardona, M.; Pollak, F. H. Stress-Induced Shifts of First-Order Raman Frequencies of Diamond- and Zinc-Blende-Type Semiconductors. *Phys. Rev. B* **1972**, *5*, 580–593.
70. Coldren, L. A.; Corzine, S. W. *Diode Lasers and Photonic Integrated Circuits*; Wiley: New York, 1995.
71. Virgilio, M.; Manganelli, C. L.; Grosso, G.; Pizzi, G.; Capellini, G. Radiative Recombination and Optical Gain Spectra in Biaxially Strained n-Type Germanium. *Phys. Rev. B* **2013**, *87*, 235313.
72. Boztug, C.; Sánchez-Pérez, J. R.; Yin, J.; Lagally, M. G.; Paiella, R. Grating-Coupled Mid-infrared Light Emission from Tensilely Strained Germanium Nanomembranes. *Appl. Phys. Lett.* **2013**, *103*, 201114.
73. Hashemi, F. S. M.; Thombare, S.; Fontcuberta i Morral, A.; Brongersma, M. L.; McIntyre, P. C. Effects of Surface Oxide Formation on Germanium Nanowire Band-Edge Photoluminescence. *Appl. Phys. Lett.* **2013**, *102*, 251122.
74. Paiella, R. Quantum Cascade Lasers. In *Comprehensive Semiconductor Science & Technology: Devices and Applications*; Bhattacharya, R., Fornari, R., Kamimura, H., Eds.; Elsevier: Amsterdam, 2011; Vol. 5.